NANO: Brief Reports and Reviews
Vol. 9, No. 1 (2014) 1450002 (12 pages)

DOI: 10.1142/S1793292014500027

INVERSION OF THE ELECTRICAL AND OPTICAL PROPERTIES OF PARTIALLY OXIDIZED HEXAGONAL BORON NITRIDE

AVINASH P. NAYAK*, ANDREI DOLOCAN†, JONGHO LEE*,
HSIAO-YU CHANG*, TWINKLE PANDHI*, MILO HOLT*,
LI TAO* and DEJI AKINWANDE*,‡

*Microelectronics Research Center
10100 Burnet Rd. Bldg 160
Austin TX 78758, USA

†Texas Materials Institute
The University of Texas at Austin
Austin, TX 78712, USA
‡deji@ece.utexas.edu

Received 11 June 2013
Accepted 12 August 2013
Published 23 September 2013

By acoustically irradiating pristine, white, electrically insulating h-BN in aqueous environment we were able to invert its material properties. The resulting dark, electrically conductive h-BN (referred to as partially oxidized h-BN or PO-hBN) shows a significant decrease in optical transmission (>60%) and bandgap (from 5.46 eV to 3.97 eV). Besides employing a wide variety of analytical techniques (optical and electrical measurements, Raman spectroscopy, SEM imaging, EDS, X-Ray diffraction, XPS and TOF-SIMS) to study the material properties of pristine and irradiated h-BN, our investigation suggests the basic mechanism leading to the dramatic changes following the acoustic treatment. We find that the degree of inversion arises from the degree of h-BN surface or edge oxidation which heavily depends on the acoustic energy density provided to the pristine h-BN platelets during the solution-based process. This provides a facile avenue for the realization of materials with tuned physical and chemical properties that depart from the intrinsic behavior of pristine h-BN.

Keywords: Hexagonal boron nitride; acoustic irradiation; sonochemistry; bandgap engineering; conductive h-BN; TOF-SIMS; partial oxidization of h-BN (PO-hBN).

1. Introduction

Recent studies have demonstrated that graphene, transition metal dichalcogenides, and other two-dimensional (2D) layered materials have great potential for the development of future advanced material systems and nanodevices.[1–6] Hexagonal boron nitride (h-BN) is one such 2D material that has stimulated extensive interest both theoretically[7–11] and experimentally.[3,12,13] This insulating, wide bandgap (∼6 eV) material is sometimes referred to as "white graphene" due to its white appearance in powder form andits hexagonal lattice structure. In

particular, h-BN has been recently investigated for its dielectric properties,[14] integration with graphene,[15] ultra-violet (UV) lasing[16] and high thermal conductivity for heat management applications.[3]

This work reports new findings in partially oxidized h-BN (PO-hBN) that reveal noticeable differences between pristine, white, electrically insulating h-BN platelets and acoustically irradiated dark, electrically conductive h-BN platelets. We focus on the analytical characterization of the material properties before and after the acoustic irradiation. The wide range of acoustic power leading to measurable changes in optical properties indicates that solution-dispersed h-BN can be used for detecting high-power acoustic events such as blasts and vibrational shocks. Based on the analytical differences between pristine and irradiated h-BN we suggest that the material inversion originates from the partial surface or edge oxidation of the initial h-BN platelets during the irradiation process. Albeit demanding continued research studies, this work presents a facile route for preparing modified h-BN nanomaterials with tunable properties for a variety of suitable applications including enhanced passive chemical sensing and blast/shock dosimeters or detectors.

2. Results and Discussion

Acoustic irradiation involves the formation and growth of microbubbles driven by acoustic energy in the liquid used as a medium for acoustic wave propagation.[17–19] The implosion of such microbubbles can lead to the generation of very high local temperature ($>5000\,\mathrm{K}$) and pressure ($>1\,\mathrm{GPa}$) conditions in very short periods of time ($\sim 2\,\mu\mathrm{s}$).[17] This can, in some cases, alter the molecular structure and composition of the solid matter dispersed in liquid.[17,19] We subject crystalline h-BN platelets (TEM image is shown in Fig. S1 in the supplementary information) to an hour of acoustic irradiation in aqueous environment which generates h-BN platelets of thinner lateral sizes and thicknesses platelets typically in the sub-10 nm range (AFM scan in Fig. S1(b) in the supplementary information). A schematic of this irradiation process is illustrated in Fig. 1(a). After the acoustic treatment a change in the appearance of the platelet powder from white to dark [see Fig. 1(b), inset] and a $\sim 60\%$ decrease in transmission [see Fig. 1(b)] are observed. We find that the transmission is heavily dependent on the ultrasonication time or acoustic energy density [see Fig. 1(c)]. The rate of change in transmission is significantly higher ($0.35\,\Delta\mathrm{T/KJcm^{-2}}$) within the first 15 min in comparison to the next 45 min of acoustic irradiation ($0.08\,\Delta\mathrm{T/KJcm^{-2}}$), which we attribute to a higher initial oxidation rate. This dependence can be useful for a range of applications including passive acoustic sensors and blast dosimeters. For instance, close-proximity blast injuries are believed to be the result from exposure

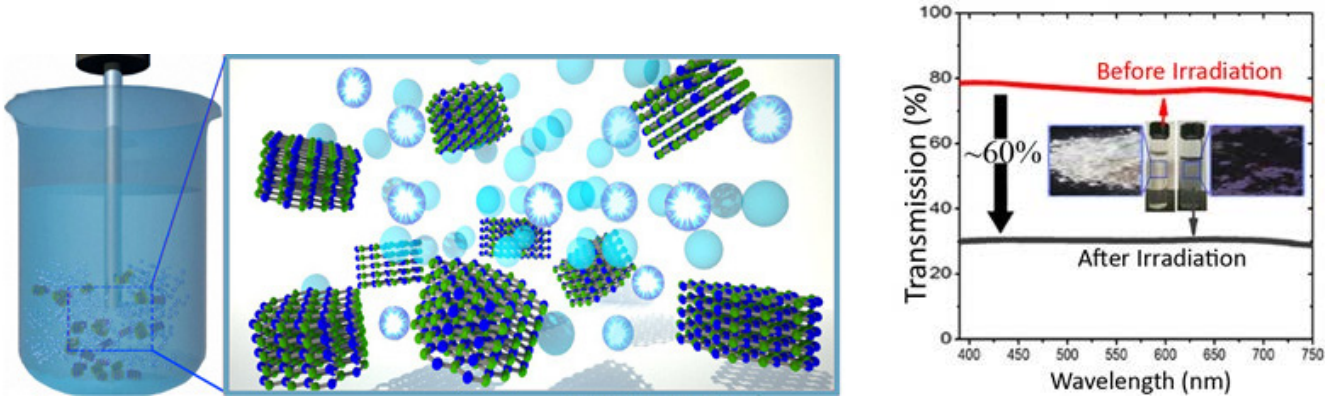

(a) (b)

Fig. 1. (a) An illustration of the growth and implosion of acoustically formed bubbles which lead to the inversion of the optical and electrical properties of h-BN flakes. (b) A large decrease in transmission is observed after 60 min of acoustic irradiation. The inset shows the optical images of h-BN in water, before and after irradiation. (c) The normalized change in the h-BN optical transmission at 500 nm wavelength reveal two regions of linear dependence. T_o is the pristine h-BN optical transmission. (d) The UV-Vis absorbance spectra of pristine h-BN (red) and after 60 min of acoustic irradiation (black). A decrease from 5.46 eV to 3.97 eV (27% decrease) in the optical bandgap is observed. (e) Upon irradiation the h-BN platelets undergo a transition from an insulating to a conductive phase (color online).

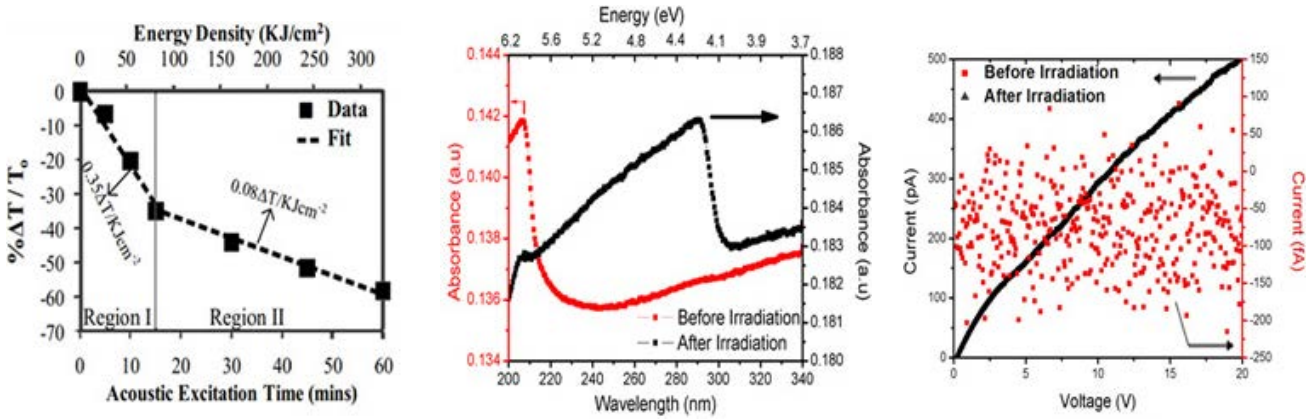

(c) (d) (e)

Fig. 1. (*Continued*)

to over pressurization wave generated by the blast itself.[20] If the blast pressure is severe enough, fluid-filled cavities such as the brain are especially susceptible to injury. Currently, photonic-nanocrystal-based blast sensors exhibit complete color loss and defragmentation when exposed to 320 kW/m^2.[21] We find that PO-hBN platelets gradually change color up to an exposure of 830 kW/m^2. This gradual color change with larger applied power density could afford for a wider range of detection for higher-intensity blasts. This dependence on irradiation energy and the change in appearance suggests that solution-dispersed h-BN or an h-BN microfluidic device might be suitable as a blast dosimeter or detector. The color change associated with the intensity provided [see Fig. 1(c)] shows that PO-hBN is highly sensitive to irradiation.

Recent theoretical and experimental studies have shown that intercalating and chemically modifying h-BN can lead to changes in appearance and conductance.[7,9,22,23] Based on the optically induced band-transition, the optical energy gap can be investigated. Figure 1(d) shows the Uv-visible (UV-Vis) absorption spectrum for pristine and irradiated h-BN. We observe a substantial (∼27%) decrease (from 5.46 eV to 3.97 eV) in the optical bandgap after irradiation due to hydroxyl (OH) ions attaching onto the irradiated h-BN platelets.[23] The optical bandgap energy was determined using Tauc's plot (see Fig. S2 in the supplementary information). Although not all the material that is obtained from the irradiation process is of the exact bandgap, a large portion of the material maintains the reduced bandgap of 3.97 eV since we observe no evidence of additional peaks in the spectroscopy. The finite conductance of PO-hBN is shown in Fig. 1(e) and reflects a transition from an insulating to a conducting phase. The presence of OH ions, and the formation of B_2O_3 during the high temperature and pressure cavitation conditions has been previously studied.[23,24] We associate the conductance of PO-hBN to the OH ions attaching onto the irradiated h-BN platelets. Mackenzie *et al.*[25] suggest that the electrical conductivity of B_2O_3 should be highly conductive ($10^{-1}\Omega m$) while we observed a highly resistive behavior (resistivity of $10^5\Omega m$). We therefore infer that if B_2O_3 played a significant effect on the conductivity, our material should have showed a highly conductive behavior. Although h-BN is considered an insulating material (E_g of 6 eV), altering the conductance of h-BN allows for the material to behave as a near-visible large bandgap semiconductor (E_g of 3.97 eV). In addition, pristine h-BN plateletsare known to be hydrophobic before irradiation.[26] We find that the PO-hBN platelets are hydrophilic (contact angle of 9°) (see Fig. 2). This is an additional evidence of the OH ions attaching onto the h-BN platelets. Previous studies reported in the literature have also observed this hydrophilicity after altering h-BN with OH groups.[27]

To understand how h-BN converts toPO-hBN, we investigated its physical and chemical structure before and after acoustic irradiation. Recent literature has reported that OH ions and H_2O_2 are formed in water while under high-intensity acoustic irradiation.[18,27] We suggest that the H_2O_2 initiates the thinning of the h-BN platelets while the OH ions attach onto the edges and surface of the PO-hBN

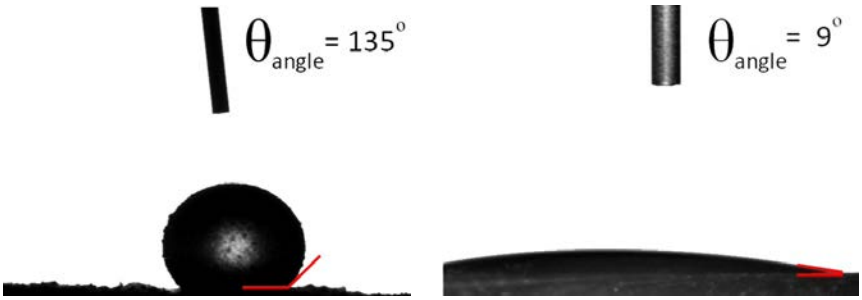

(a) (b)

Fig. 2. (a) Pristine h-BN platelets are observed to have a contact angle of 135° while the (b) contact angle for PO-hBN is 9°. This reduction of hydrophobicity is attributed to hydroxyl ions on the surface of the irradiated h-BN. This suggests that OH ions would likely promote the hydrophilicity to h-BN after irradiation (color online).

platelets. To examine if OH ions are attached to the surface, we employ Fourier transform infrared (FTIR) spectroscopy to observe the O–H vibration mode at 3435 cm^{-1} (see Fig. S3 in the supplementary information). To find the difference in percentage composition of oxygen and to determine the elemental bonding to the oxygen species, we employed X-ray photoelectron spectroscopy (XPS). As shown in Fig. 3(a), we find that the surface coverage with oxygen species increases from 2% to 41% (based on the O1s peaks) signifying a substantial increase upon acoustic irradiation. Additionally, the B1s peak for the PO-hBN, has a small shoulder at 192 eV binding energy, corresponding to the B1s core level shift due to a B–O bond (see Fig. S4 in the supplementary information).

As suggested by the BN phase diagram,[28] synthesis at different pressures and temperatures can lead to w-BN (wurtzite boron nitride), c-BN (cubic boron nitride), r-BN (rhombohedral boron nitride) or h-BN. To elucidate any changes to the crystal structure, we examine the pristine and irradiated platelets using Raman and X-ray diffraction (XRD) spectroscopy [see Figs. 3(b) and 3(c) respectively]. We find that the intrinsic h-BN E_{2g} vibrational mode (at 1367 cm^{-1}) did not change after irradiation [see Fig. 3(b)]. The XRD however, indicates the presence of β-B_2O_3 (boron trioxide)[29] crystalline phase in the PO-hBN [see Fig. 3(c)], which is not surprising since sintering boron nitride in water leads to the formation of B_2O_3 and NH_3.[24,30,31] In order to confirm the presence of ammonia, we use Nessler's reagent (a K_2HgI_4/KOH solution) and observe a yellow coloration which is an indicator of the presence of NH_3.[27] It has been reported by Shen *et al.*[22] that intercalation of h-BN

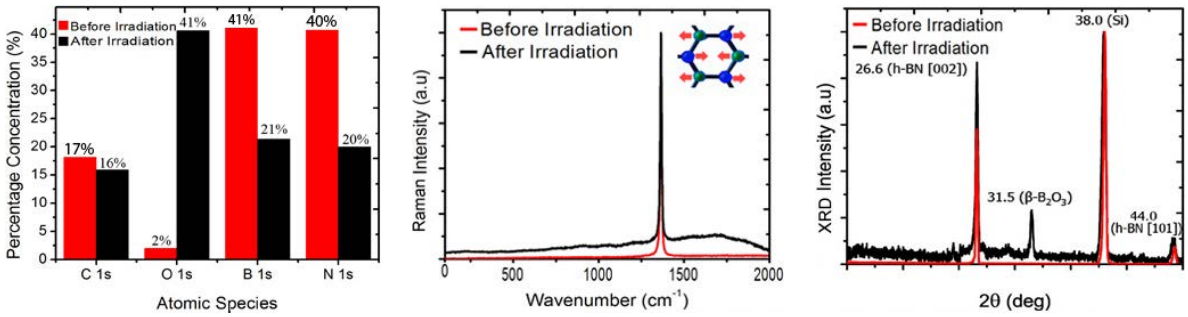

(a) (b) (c)

Fig. 3. (a) XPS elemental percentage concentration of various atomic species. The oxygen surface concentration increases from 2% to 41% after irradiation. (b) The Raman peak at 1367 cm^{-1} is observed before and after acoustic irradiation indicating that the crystallinity remains hexagonal. The inset depicts the E_{2g} phonon mode responsible for the Raman peak. (c) XRD shows the β-B_2O_3 peak for the irradiated h-BN which likely arises from the oxidation of h-BN during the high temperature/pressure cavitation conditions. SEM image and SEM–EDS spectra of (d) individual pristine h-BN platelet and (e) PO-hBN platelet after acoustic irradiation. The energy peaks for N (at 0.2 KeV) and B (at 0.4 KeV) are observed both before and after h-BN irradiation, but O (at 0.55 KeV) is detected only in PO-hBN (color online).

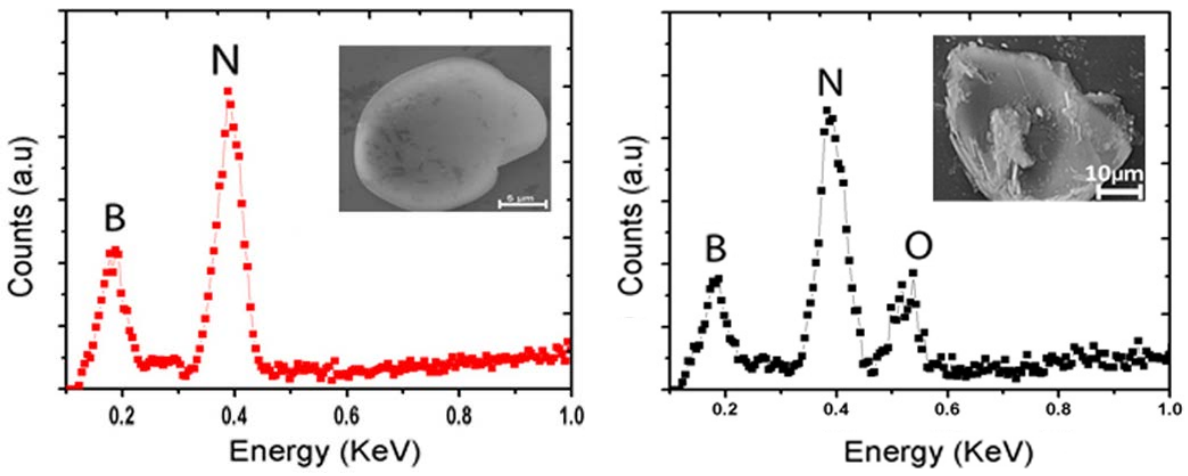

(d) (e)

Fig. 3. (*Continued*)

by SO_3F not only alters the color (from white to deep blue) of the material, but also changes the electrical conductivity (from 1.5 $S \cdot cm^{-1}$ to $1.1 \times 10^5\, S \cdot cm^{-1}$). We attribute the change in color observed in our results to the partial oxidization of h-BN caused by the acoustic energy density provided to the solution. In evidence of this, energy dispersive X-ray spectroscopy (EDS) was employed to detect the presence of oxygen in the irradiated h-BN [see Fig. 3(e)]. EDS-mapping of oxygen, boron and nitrogen species were done on both pristine and irradiated samples showing that oxygen species is prevalent after irradiation (see Fig. 4).

In order to locate and identify qualitatively and quantitatively the species of interest (OH, BO) on both pristine and irradiated h-BN platelets, we employ TOF-SIMS, a highly surface-sensitive (sensitivity in the parts-per-billion range) analytical technique.[32] TOF-SIMS is employed with the purpose of (i) detecting changes in chemical composition and (ii) relative quantification of species of interest between the pristine h-BN and PO-hBN.

We first focus on identifying the chemical changes that occur at the very surface of the irradiated h-BN. For PO-hBN [see Fig. 5(a)] a consistent increase in the OH amount, $\frac{\left[\left(\sum_m I_{OH}\right)/\left(\sum_m I_B\right)\right]_{irradiated}}{\left[\left(\sum_m I_{OH}\right)/\left(\sum_m I_B\right)\right]_{pristine}} \cong 4$, where I_M defines the secondary ion (SI) intensity of the detected species M while $\sum_m I_M$ indicates the total SI count of species M spanning a mass range m (i.e., the total count of the SI peak), was observed together with an even larger increase in BO amount, $\frac{\left[\left(\sum_m I_{BO}\right)/\left(\sum_m I_B\right)\right]_{irradiated}}{\left[\left(\sum_m I_{BO}\right)/\left(\sum_m I_B\right)\right]_{pristine}} \cong 10$. These ratios

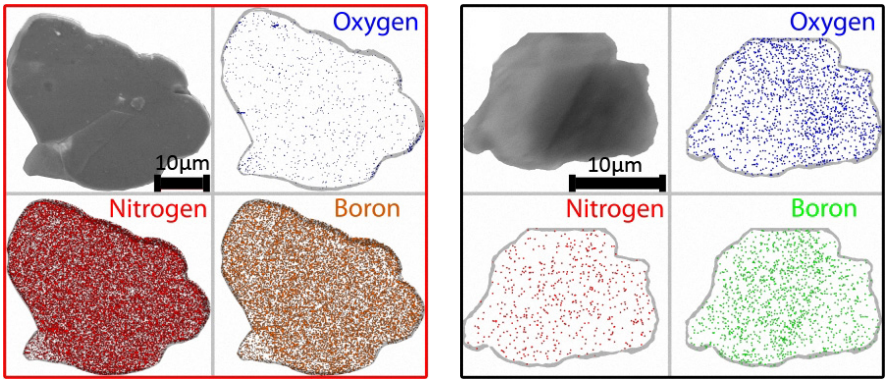

(a) (b)

Fig. 4. SEM–EDS mapping of oxygen, nitrogen and boron in (a) pristine h-BN and (b) PO-hBN after 60 min of irradiation. The presence of oxygen species is evident in the EDS mapping of PO-hBN.

(normalized to boron to account for surface area and matrix changes) imply that the surface of the h-BN platelets is oxidizing upon ultrasound irradiation in aqueous solution. To further localize the extent of the surface oxidation we make use of the TOF-SIMS' BA mode (high spatial resolution, $\sim$200 nm). Figures 5(b) and 5(c) present the actual surface distribution of B, BO and OH. While the high-resolution map of the pristine h-BN shows the OH and BO species located mostly at the platelets' boundaries, the map of the PO-hBN indicates that the OH and BO species are essentially covering most of the platelets' surfaces. Associated with the high concentration increase in OH and BO species upon irradiation, the reduction of the platelets size implies that during the acoustic irradiation process the h-BN platelets experience simultaneous fragmentation and oxidation. Furthermore, due to the B_2O_3 signal present in the PO-hBN TOF-SIMS spectra, combined with XRD measurements shown in Fig. 5(c), we summarize that the detected BO signal is, in fact, a marker for the parent B_2O_3 molecule.

Figures 5(a)–5(c), are taken in Static SIMS mode where only a few of the outermost layers are probed. It is of interest, however, to know the chemical differences as function of surface depth by looking at the species of interest (OH and BO) as function of sputtering time (i.e., depth profiling). First, the OH and BO depth profiles for the irradiated sample should indicate both the mechanism and penetration depth of oxidation in the PO-hBN flakes. Second, the ratio between the depth profile of OH (or BO) species for the irradiated sample and the corresponding depth profile of OH (or BO) species for the pristine sample should indicate the relative increase in OH (or BO) amount as function of depth as a result of the acoustic treatment.

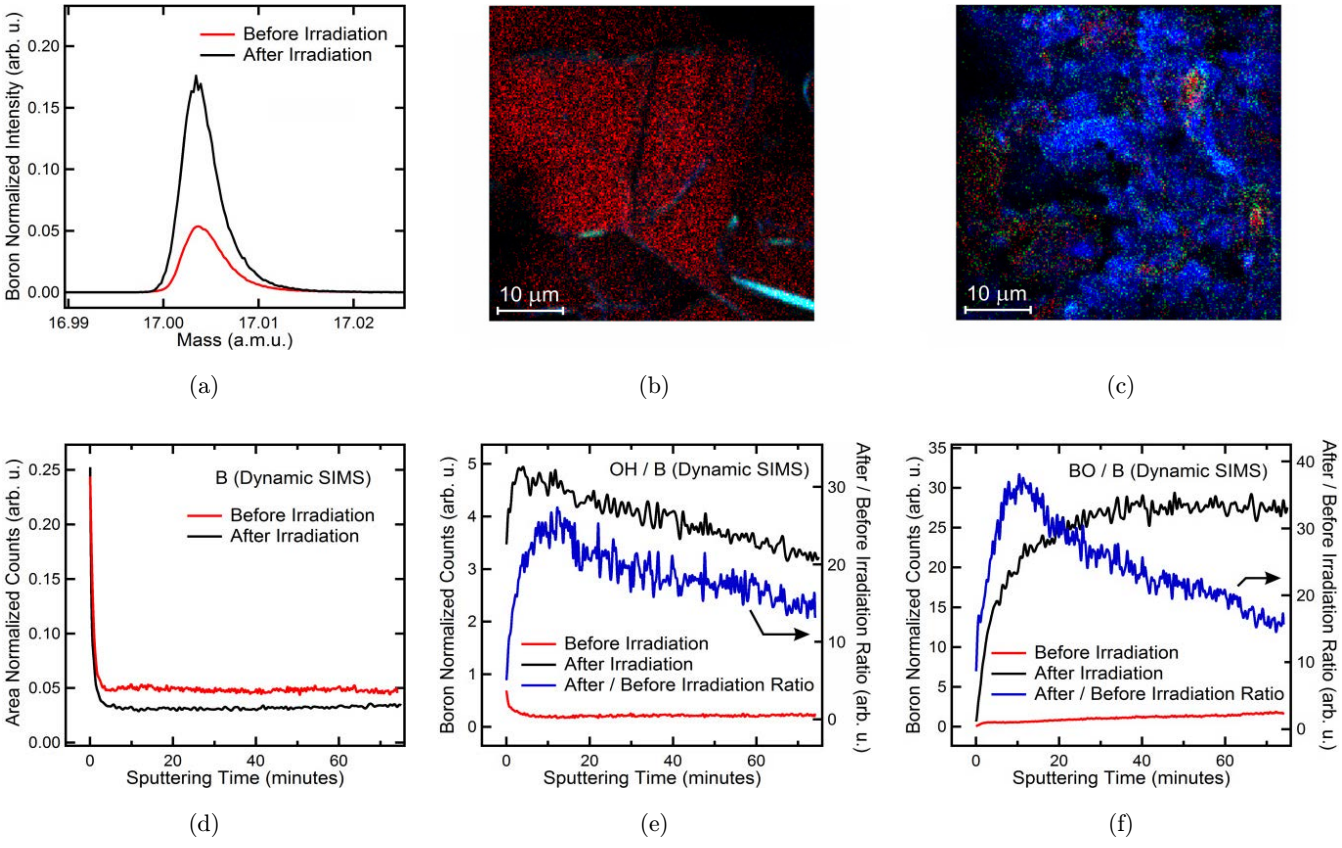

Fig. 5. (a) Comparison of the OH signal normalized to the total boron count for pristine and irradiated h-BN samples. (b) Overlay of B (red), BO (green) and OH (blue) signals for the pristine and (c) irradiated h-BN sample. The irradiated h-BN platelets reveal coverage by OH species. (d) Dynamic SIMS depth profiles of the boron signal normalized to its coverage area for the pristine (red curve) and irradiated (black curve) h-BN. A steady state is reached after 5–10 min of sputtering. Dynamic SIMS depth profiles of the (e) OH and (f) BO signals normalized to their corresponding B signals for pristine (red curve) and irradiated (black curve) h-BN. The ratios of the irradiated and pristine curves in each plot are shown in blue (color online).

In Fig. 5(d), we present the Dynamic SIMS depth profiles of boron, $\sum_m I_B(t)$, where t is the Bi_1^+ sputtering time, normalized to their region of interest areas, for both pristine and irradiated samples. These depth profiles are used as reference curves for the other species of interest to account for surface area and matrix changes, as shown in Figs. 5(e) and 5(f) where the OH and BO depth profiles, respectively, are normalized to their corresponding B depth profile (black and red curves). First, we observe that the actual BO signal (referenced to boron) reaches saturation after 40 min to 50 min of sputtering [see Fig. 5(f), black curve] while the corresponding OH signal [see Fig. 5(e), black curve] starts decaying almost immediately from the surface. This suggests that the OH radicals penetrate the surface during the irradiation process and start generating B_2O_3 at a rate that depends on depth, We think that as the pressure exerted between atomic layers is increasing with depth, the OH radicals convert more into β-B_2O_3 packing thus the inverse proportionality between the OH and BO depth profiles [see black curves in Figs. 5(e) and 5(f), respectively].

Second, the relative ratios (irradiated vs pristine) of both OH and BO profiles [see blue curves in Figs. 5(e) and 5(f), respectively] indicate that the relative amount increase in OH and BO species is a function of depth which reaches a maximum after about 10 min of sputtering. We find that, for both species, the increase factor maximum is about 5 times larger than its value at the very surface (which was also calculated above from the Static SIMS data), suggesting that the main chemical differences between PO-hBN and pristine h-BN samples are located in the first few nanometers of the surface. Since the OH and BO relative depth profiles [see blue curves in Figs. 5(e) and 5(f), respectively] are very similar, we consider that these curves are most indicative of the actual chemistry responsible for the dramatic changes in physical properties following the acoustic treatment.

Our investigation demonstrates that the observed properties of PO-hBN material are caused by both the presence of OH ions and boron oxidation of the surface. EDS, XPS and TOF-SIMS coherently show a magnitude increase in the amount of oxygen per detected boron signal. Although the crystal structure remains virtually the same for both h-BN and PO-hBN flakes, a significant 27% decrease in the optical bandgap and a significant increase in conductance are observed in the acoustically irradiated h-BN flake. Having precise control over the bandgap and altering surface conduction warrants more investigations on PO-hBN. Future systematic studies on enhancing the material properties of h-BN are expected to enable further understanding and material control leading toward advanced tunable nanomaterials and enhanced sensors.

ASSOCIATED CONTENT

TEM, Tauc's Plots, FTIR, XPS, and further discussion on the acoustic irradiation settings and TOF-SIMS is available free of charge via the Internet at http://pubs.acs.org.

Author Contributions

The manuscript was written through contributions of all authors. All authors have given approval to the final version of the manuscript.

Funding Sources

We acknowledge the NSF grants DMR-0923096 and DMR-0618242. This work was supported in part by the Defense Threat Reduction Agency, Basic Research Award # HDTRA1-10-9-8996, to University of Texas, Austin.

3. Methods

Hexagonal boron nitride (from Momentive, PT110) was used without further purification. Approximately 3.5 mmol of h-BN was ultrasonicated using the VCX 650X (Sonics & Materials) for 60 min (see Supplementary information for more details).

All samples were imaged using a Quanta 650 FEG FE-SEM with EDS capability. Cary 5000 UV-Vis NIR Spectrometer was used to obtain the optical absorbance curves. The electrical measurements (Cascade B1500/Agilent 4156C semiconductor perimeter analyzer) along with XRD (Philips X'Pert Pro X-ray system) were done at room ambient conditions. The SEM–EDS, XPS and TOF–SIMS measurements were performed in ultra-high vacuum (UHV) on h-BN platelets that were dispersed on a 40 nm Au-coated Si substrate. The acquisition time for each SEM–EDS profile was 3 min with the same working distance for all samples.

XPS spectra were recorded using a commercial X-ray photoelectron spectrometer (Kratos Axis Ultra, 2007). The detection angle of photoelectrons was normal to the sample surface and 45° with respect to the X-ray beam (Al Kα; hν = 1486.5 eV). The pressure in the analysis chamber was typically

4×10^{-9} Torr during data acquisition. Casa XPS analysis software was used for peak analysis.

A time-of-flight secondary ion mass spectrometer (TOF.SIMS5 by ION-TOF GmbH, 2010) was used for chemical surface analysis. When probing the sample surface the TOF-SIMS primary ion gun, shooting 18 ns Bi_1^+ ion pulses at 30 kV energy, was set in one of the two main modes: (1) high current (HC) Bunched mode (2.8 pA beam current), which allows for high-mass resolution ($m/\delta m > 8000$ for all analyzed masses) but only average lateral resolution ($\sim$1–2 μm), or (2) Burst Alignment (ba) mode (0.04 pA beam current) which allows for both high-mass and lateral resolution ($\sim$200 nm). Most of the data was acquired in HC mode with the primary beam raster-scanning areas of either $100 \times 100\,\mu m^2$, for analysis of the outermost surface layer (i.e., Static SIMS), or $20 \times 20\,\mu m^2$, for shallow depth profiling (i.e., Dynamic SIMS). The BA mode was used to identify the location of interesting species on areas of $50 \times 50\,\mu m^2$ with high lateral resolution. All data were acquired in negative secondary ion detection mode (i.e., all secondary ions detected had negative polarity) and with a low-energy (21 eV) electron beam flooding the sample for charge compensation. All HC mode data were reconstructed from the initial TOF-SIMS data files such that only the h-BN covered part of the scanned area is taken into account. In order to eliminate surface contamination due to sample exposure to air, both samples (pristine and irradiated h-BN) were annealed at 120°C for 15 min under UHV before surface analysis for both XPS and TOF-SIMS.

Acknowledgment

We would like to thank Dr. Sushant Sonode, Harry Chou, Dr. Ariel Ismaj and Michael Ramon for their helpful discussions. Donghyi Koh, Nassibe Rahimi and Maria Michael for their help with the deposition of metal. We are grateful to Prof. Rod Ruoff for providing the acoustic irradiation tool.

References

1. A. K. Geim and K. S. Novoselov, *Nat. Mater.* **6**, 183 (2007).
2. K. S. Novoselov, D. Jiang, F. Schedin, T. J. Booth, V. V. Khotkevich, S. V. Morozov and K. Geim a, *Proc. Natl. Acad. Sci. USA* **102**, 10451 (2005).
3. J. Taha-Tijerina, T. N. Narayanan, G. Gao, M. Rohde, D. A. Tsentalovich, M. Pasquali and P. M. Ajayan, *ACS Nano* **6**, 1214 (2012).
4. H. Wang, T. Taychatanapat, A. Hsu, K. Watanabe, T. Taniguchi, P. Jarillo-Herrero and T. Palacios, *IEEE Electron Device Lett.* **32**, 1209 (2011).
5. Z. Yin, H. Li, L. Jiang, Y. Shi, Y. Sun and G. Lu, *ACS Nano* **6**, 74 (2011).
6. L. Tao, J. Lee, H. Chou, M. Holt, R. S. Ruoff and D. Akinwande, *ACS Nano* **6**, 2319 (2012).
7. A. Lopez-Bezanilla, J. Huang, H. Terrones and B. G. Sumpter, *Nano Lett.* **11**, 3267 (2011).
8. V. Barone and J. E. Peralta, *Nano Lett.* **8**, 2210 (2008).
9. M. Terrones, J.-C. Charlier, A. Gloter, E. Cruz-Silva, E. Terrés, Y. B. Li, A. Vinu, Z. Zanolli, J. M. Dominguez, H. Terrones, Y. Bando and D. Golberg, *Nano Lett.* **8**, 1026 (2008).
10. L. Chkhartishvili, *Mater. Sci. Appli.* **01**, 222 (2010).
11. K. Oda and T. Y. Oshio, *Ind. Chem.* **28**, 6562 (1993).
12. L. Song, L. Ci, H. Lu, P. B. Sorokin, C. Jin, J. Ni, A. G. Kvashnin, D. G. Kvashnin, J. Lou, B. I. Yakobson and P. M. Ajayan, *Nano Lett.* **10**, 3209 (2010).
13. Z. Liu, L. Song, S. Zhao, J. Huang, L. Ma, J. Zhang, J. Lou and P. M. Ajayan, *Nano Lett.* **11**, 2032 (2011).
14. G.-H. Lee, Y.-J. Yu, C. Lee, C. Dean, K. L. Shepard, P. Kim and J. Hone, *Appl. Phys. Lett.* **99**, 243114 (2011).
15. C. R. Dean, A. F. Young, I. Meric, C. Lee, L. Wang, S. Sorgenfrei, K. Watanabe, T. Taniguchi, P. Kim, K. L. Shepard and J. Hone, *Nat. Nanotechnol.* **5**, 722 (2010).
16. Y. Kubota, K. Watanabe, O. Tsuda and T. Taniguchi, *Science (New York, NY)* **317**, 932 (2007).
17. K. Suslick, *Scientific American* **260**, 2 (1989).
18. K. S. Suslick, *Science* **247** (1990).
19. W. B. M. Iii, Y. T. Didenko and K. S. Suslick, **401**, 4 (1999).
20. D. K. Cullen, K. D. Browne, Y. Xu, S. Adeeb, J. A. Wolf, R. M. McCarron, S. Yang, M. Chavko and D. H. Smith, *J. Neurotrauma* **28**, 2307 (2011).
21. D. K. Cullen, Y. Xu, D. V. Reneer, K. D. Browne, J. W. Geddes, S. Yang and D. H. Smith, *NeuroImage* **54**, S37 (2011).
22. C. Shen, S. Mayorga and R. Biagioni, *J. Solid State Chem.* **147**, 74 (1999).
23. T. Oku, M. Kuno, H. Kitahara and I. Narita, *Int. J. Inorg. Mater.* **3**, 597 (2001).
24. V. V. Brazhkin, Y. Katayama, Y. Inamura, M. V. Kondrin, A. G. Lyapin, S. V. Popova and R. N. Voloshin, *J. Exp. Theor. Phys. Lett.* **79**, 308 (2004).
25. J. D. Mackenzie, *Trans. Faraday Soc.* **52**, 1564 (1956).

26. C. Lee, J. Drelich and Y. Yap, *Langmuir* **25**, 4853 (2009).
27. Y. Lin, T. V. Williams, T.-B. Xu, W. Cao, H. E. Elsayed-Ali and J. W. Connell, *J. Phys. Chem. C* **115**, 2679 (2011).
28. V. L. Solozhenko, V. Z. Turkevich and W. B. Holzapfel, *J. Phys. Chem. B* **103**, 2903 (1999).
29. V. Mukhanov, *J. Superhard Mater.* **30**, 71 (2008).
30. Y. Chen, J. Zou, S. J. Campbell and G. Le Caer, *Appl. Phys. Lett.* **84**, 2430 (2004).
31. T. Saito and F. Honda, *Wear* **237**, 253 (2000).
32. J. C. Vickerman, Secondary ion mass spectrometry–basic concepts, instrumental aspects, applications and trends. in Surface and Interface Analysis, eds. A. Benninghoven, F.G. Rudenauer and H. W. Werner (Wiley, New York, 1987), p. 1277.

Supporting Information

Acoustic irradiation settings

The important factors to consider for reproducible results are frequency and power of acoustic waves, time of irradiation, solution temperature, type of solution, beaker diameter, ultrasonic probe tip/horn and reaction environment. In this study, we find that using 90 W·cm^{-2} at 20 kHz (an average of 130 W), 60 min of irradiation (in a 200 mL beaker with a 1 inch diameter), 1 cm above the base of the beaker, at room ambient conditions in aqueous solution of 3.5 mMol of h-BN platelets gives us >90% h-BN platelets that are dark.VCX 650X (with a horn tip diameter of 1.3 cm) from Sonics and Materials was used to acoustically irradiate h-BN platelets with the specifications stated above.

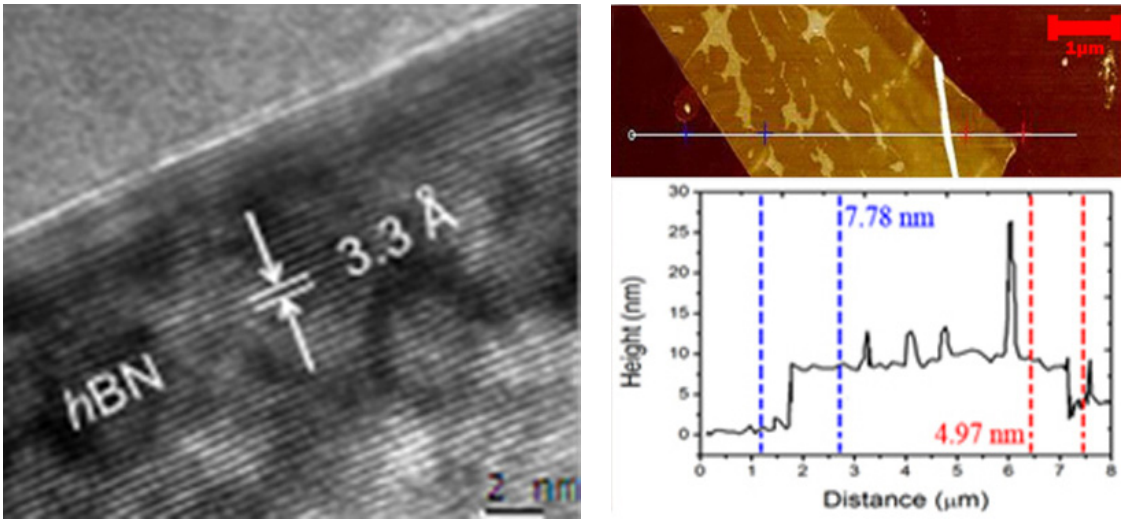

(a) (b)

Fig. S1. (a) The TEM cross section of a pristine h-BN platelet. The measured interlayer lattice spacing is 3.3 Å in agreement with expectations. (b) AFM image of the PO-hBN flakes which shows the thickness of the exfoliated flakes are in the sub-10 nm (∼20 layers of h-BN) range (color online).

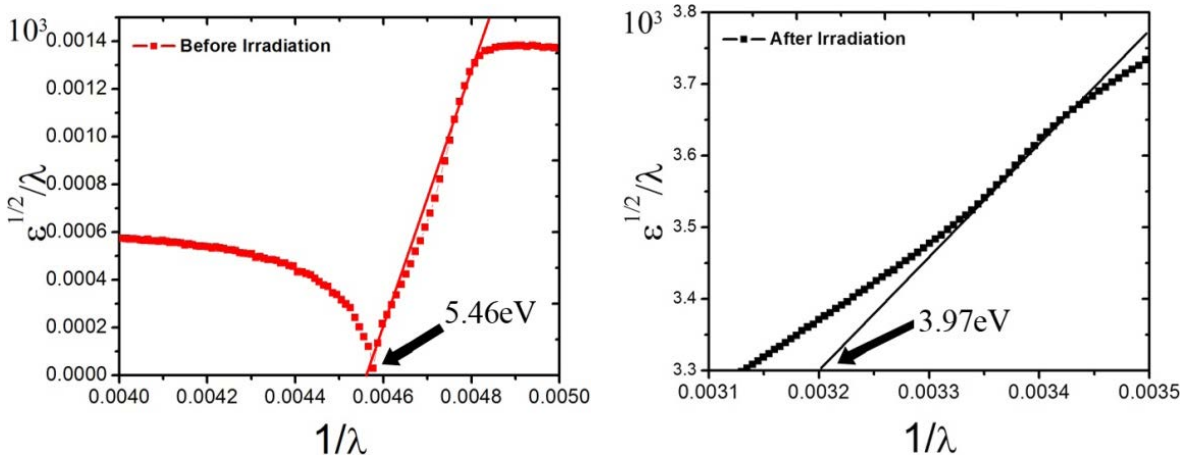

(a) (b)

Fig. S2. Tauc's plot of (a) pristine h-BN indicates an optical bandgap of 5.46 eV while (b) acoustically irradiated h-BN reveals a bandgap of 3.97 eV. A decrease from 5.46 eV to 3.97 eV (27% decrease) in the bandgap is observed.

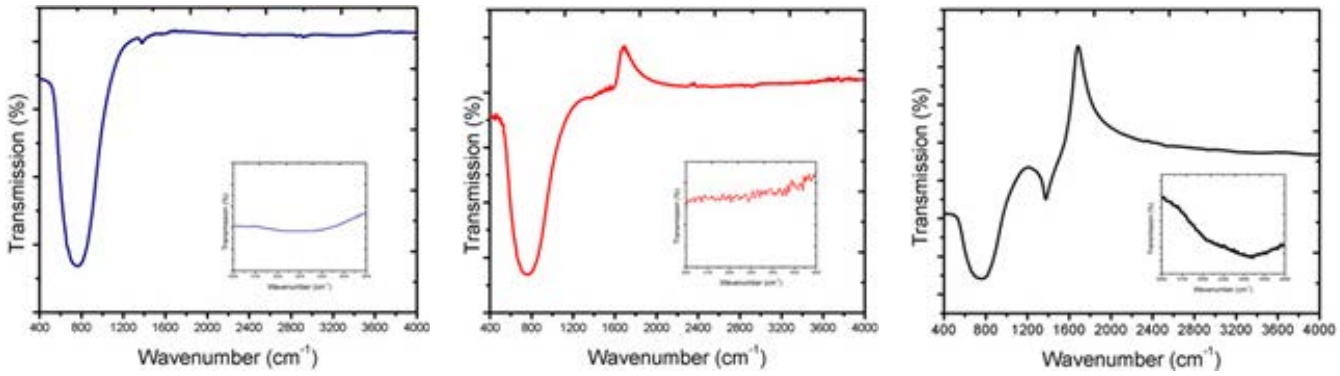

(a) (b) (c)

Fig. S3. (a) FTIR peaks at $\sim$800 cm^{-}1 and $\sim$1300 cm^{-1} is attributed to h-BN. (b) FTIR peaks from the pristine h-BN powder (c) FTIR peaks from the irradiated h-BN. The OH peak is detected at 3435 cm^{-1} only in the PO-hBN platelets.

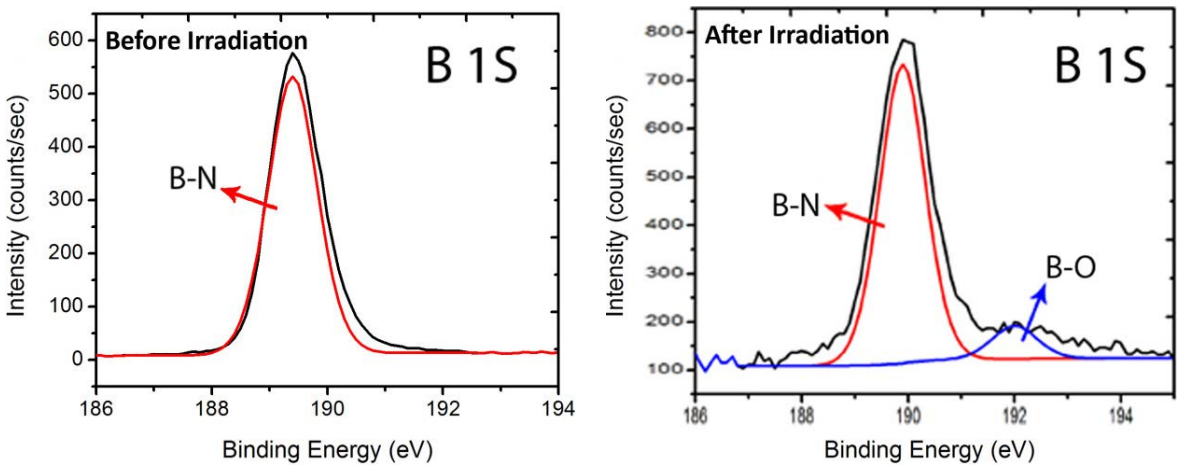

(a) (b)

Fig. S4. (a) B1s XPS spectrum for pristine h-BN platelets. (b) B1s peak for PO-hBN. The B1s peak at 192 eV corresponding to a B–O bond along with the B1s corresponding to a B–N peak at 190 eV is observed. This B–O peak is not observed in pristine h-BN (color online).

TOF-SIMS:

Designed as a method to interrogate the outermost molecular (or atomic) layers (few Angstroms) [TOF1][TOF2] of solid surfaces, TOF-SIMS not only determines the presence of chemical species at the surface but also divulges information regarding the chemical composition of the species being investigated. Absolute quantification of interesting species is not generally possible with TOF-SIMS due to variations in the secondary ion signal generated from the same species located in different matrices (i.e., chemical environments). [TOF3] However, relative quantification based on reference samples (i.e., samples that maintain as much as possible the matrix of the sample under investigation and contain the species of interest at TOF-SIMS detectable levels) is possible. Furthermore, if the interesting species in the reference sample have a known concentration one can determine their absolute concentration in other samples that have an identical or similar matrix. In our case, TOF-SIMS is employed with the purpose of (1) detecting changes in chemical composition and (2) relative quantification of species of interest between the pristine and irradiated h-BN. An absolute determination of the interesting species' concentration is not important as we interrogate the relative chemical difference resulting from treating the h-BN flakes.

Based on HC data recorded from $100 \times 100\,\mu$m^2 areas in eight random locations, in average, the total

count of OH to B ratio reads 1.29 ± 0.32 for the pristine (i.e., $[(\sum_m I_{\mathrm{OH}})/(\sum_m I_{\mathrm{B}})]_{\mathrm{pristine}}$, where $\sum_m I_{\mathrm{OH}}$ and $\sum_m I_{\mathrm{B}}$ define the total detected counts for the OH and B secondary ions, respectively; the summation indicates the secondary ion count integration over the mass) and 4.34 ± 0.75 for the irradiated (i.e., $[(\sum_m I_{\mathrm{OH}})/(\sum_m I_{\mathrm{B}})]_{\mathrm{irradiated}}$) sample. These values were extracted from the initial TOF-SIMS data files that were reconstructed by using regions of interest comprising only the h-BN covered part of the scanned area (i.e., we kept only the area that showed no signal originating from the gold substrate). Moreover, the average carbon to boron ratio for pristine and irradiated h-BN was found to be 1.34 ± 0.24 and 0.96 ± 0.17, respectively, at the same locations. The relatively close values for the two C to B ratios indicate that the annealing process leaves a similar amount of contamination on both samples.

Depth profiles can be acquired in either Static or Dynamic SIMS mode by using a secondary ion gun for the actual surface sputtering together with the primary ion gun for surface probing or only the primary ion gun which can sputter while probing the sample, respectively. While the Static SIMS depth profiling can interrogate a larger surface depth (up to hundreds of nanometers to few microns per hour) due to the far higher sputtering current yielded by the secondary ion gun with respect to the primary ion gun, the Dynamic SIMS depth profiling can penetrate the surface only a few nanometers (about 5–10 nm in our case) [TOF4] in an hour for most solid materials. However, the Dynamic SIMS profiling has virtual atomic resolution due to slow sputtering rates. For our particular case, another advantage of the Dynamic over the Static SIMS depth profiling is that when dealing with relatively soft powders the strong sputtering beam currents used in Static SIMS depth profiling can remove completely the particles from the surface under investigation during data acquisition. This effect, which induces unwanted artifacts in the depth profile, can be avoided by using the small sputtering currents of the primary ion gun in the Dynamic SIMS mode.

References for Supporting Information

1. R. Behrisch and W. Eckstein, Results of molecular dynamics calculations, in *Sputtering by Particle Bombardment* (Springer-Verlag, 2007), p. 191.
2. Th. J. Colla and H. M. Urbassek, *Nucl. Instrum. Methods Phys. Res. B* **152**, 459 (1999).
3. H. Gnaser, *Phys. Rev. B* **63**, 045415 (2001).
4. K.-S. Park, P. Xiao, S.-Y.Kim, A. Dylla, Y.-M. Choi, G. Henkelman, K. J. Stevenson and J. B. Goodenough, *Chem. Mater.* **24**, 3212 (2012).